JOURNAL OF SPACECRAFT AND ROCKETS
Vol. 60, No. 6, November–December 2023

Generation of Multiple-Revolution Many-Impulse Optimal Spacecraft Maneuvers

Vishala Arya*
Texas A&M University, College Station, Texas 77843-3141
Keziban Şaloğlu† and Ehsan Taheri‡
Auburn University, Auburn, Alabama 36849
and
John L. Junkins§
Texas A&M University, College Station, Texas 77843-3141

https://doi.org/10.2514/1.A35638

Impulsive trajectories provide time- and ΔV-reachability insights. Two novel homotopy-based methods are proposed for generating optimal many-impulse, multirevolution maneuvers. The first method is based on the continuation over the specific impulse value, which is shown to enhance convergence performance of the resulting two-point boundary-value problems. The second method is based on the formulation of impulsive trajectories using a linear acceleration term. The two methods are used in a hybrid framework. The utility of the proposed methods is demonstrated on four problems: Two interplanetary trajectories 1) from Earth to Mars, 2) from Earth to asteroid Dionysus, 3) a planet-centric transfer maneuver from a geostationary transfer orbit (GTO) to geostationary orbit (GEO) consisting of 21 revolutions, and 4) a 50-revolution transfer from the considered GTO to a circular orbit at the first Lagrange point (L1) of the Earth–moon system. The last two problems leading to 18 and 50 impulses are tackled to give an optimal near-impulsive solution. The impulsive solution with 18 impulses is shown to satisfy Lawden's conditions.

I. Introduction

IMPULSIVE maneuvers hold a special place within reachability analysis studies and preliminary design phases of space missions [1,2] as well as uncertainty propagation analysis [3]. More specifically, impulsive maneuvers provide theoretical limits for minimum-time and minimum-fuel extremals. For realizing impulsive maneuvers, a search for the optimal number, time instants, magnitude, and direction of the velocity impulses is carried to accomplish general three-dimensional multiple-revolution orbit transfers while minimizing the total ΔV [4]. The earliest efforts in finding the optimal impulsive solutions were by Lawden, culminating in Lawden's necessary conditions [5] along with the works by Edelbaum [6] under an inverse-square gravity model.

Traditional methods for finding minimum-ΔV trajectories typically use an interactive method [7] and rely on parameter optimization and transcription methods. The methods keep improving the number, estimated times, directions, and magnitudes of the impulses in an iterative manner. For trajectories that consist of N impulses, optimization over a $4N$ dimensional search space has to be performed (i.e., for each impulse, the position vector and the time of the impulse make four unknowns). However, the search space is riddled with local extrema with no guaranteed unimodal performance hypersurface.

Recent efforts have extended the classical impulsive work to include restricted three-body dynamics [8] and solve multi-impulse multiple gravity assists problems [9]. A review of the trajectory optimization methods is given in [10].

Finding optimal multi-impulse, minimum-ΔV trajectories can become quite challenging for a number of reasons:

1) Gradient-based solvers may face difficulty in finding an optimal solution unless started with high-quality initial guesses.

2) The performance of the evolutionary algorithms depreciates as the number of design variables increases.

3) Direct methods struggle to optimize multirevolution trajectories, where the bulk of the initial transfer orbits occur near the attracting center [11].

4) Ambiguity in the optimal number of impulses further increases the problem complexity. Additionally, the solution can be nonunique if the number of revolutions is also considered as a decision variable [12].

The above-mentioned difficulties are still relevant for any method that is used for obtaining optimal impulsive solutions. Especially, when multiple orbital revolutions are involved, the complexity and nonuniqueness of the solution space introduce further difficulty in the formulation of the multi-impulse, minimum-ΔV trajectory optimization problem.

Historically, indirect methods have also been either too cumbersome to converge, leading to challenging optimization problems as the number of impulses grows into double digits or have suffered from multiple closely located or nonunique solutions [8,13]. Thus, direct optimization methods are used more extensively [14–16]. Recently, Taheri and Junkins [12] introduced the concept of *optimal switching surfaces* and answered Edelbaum's question [6] with a surprising finding that there does not always exist a unique optimal solution. However, their proposed methodology required information about thrust magnitude, the specific impulse of the propulsion system, as well as the mass of the spacecraft, which are necessary for constructing low-thrust, fuel- and time-optimal trajectories. A part of this work is introduced in [17], involving only the acceleration-based formulation with an extension to the restricted three-body world presented by Saloglu and Taheri [18].

The approach proposed in this paper draws its motivation from the ones presented in [12]; however, we propose a set of advancements to facilitate and accelerate the numerical solution procedure by devising

Presented as Paper 21-399 at the 31st AAS/AIAA Space Flight Mechanics, Virtual Meeting, Charlotte, NC, February 1–4, 2021; received 8 December 2022; revision received 12 April 2023; accepted for publication 17 April 2023; published online 12 June 2023.

*Postdoc, Department of Aerospace Engineering; varya@tamu.edu (Corresponding Author).

†Ph.D. Student, Department of Aerospace Engineering. Student Member AIAA.

‡Assistant Professor, Department of Aerospace Engineering. Senior Member AIAA.

§Distinguished Professor, Department of Aerospace Engineering. Honorary Fellow AIAA.

a novel robust two-step process to generate many-impulsive minimum-ΔV solutions. Near-impulsive solutions provide high-quality initial guesses for the position, time, direction, and magnitude of impulses, which can be used by a gradient-based solver to recover the precise impulsive solution that obeys Lawden's optimality conditions. The key to this approach, as is well known, is recognizing that impulsive trajectories can be rigorously viewed as the limiting case of high-acceleration trajectories. The standard methods that use acceleration vector construct a quadratic cost functional. However, it is important to devise a mechanism to not only enforce the so-called "bang-off-bang" profiles on the acceleration arcs, but also ensure that the thrust acceleration arcs occur over short time intervals [19]. Thus, a solution to the minimized-acceleration-integral problem, where the thrust acceleration arcs are represented as small finite burn sequences, can approximate the optimal impulsive trajectories as the thrust acceleration magnitude approaches infinity.

The contribution of the paper is to use both specific impulse and acceleration-based method in a synergistic way to generate many-impulse solutions in a robust manner. While the methods individually share the same drawbacks and difficulties common with the traditional methods used in the literature, the two-step process seeks to address some of the associated challenges with generating multi-impulse solutions. Especially, since the solution is not unique for the same transfer, the method delivers only a subset of the optimal impulsive maneuvers. The implementation of the two methods and a hybrid two-step optimization framework are given in great detail. The minimized-acceleration-integral formulation removes the dependency of the problem formulation on mass, specific impulse, and thrust value.

While acceleration-based method offers advantages by simplifying the problem, our experience is that the solution procedure can be made more fast and robust if a two-step solution procedure, such as the one presented here, is adopted. It is well established that formulation of a minimum-fuel problem using the variable-specific-impulse, variable-thrust (VIVT) propulsion model has a broader domain of convergence compared to a pure acceleration-based formulation. However, to achieve a near-impulsive solution, it is necessary to perform numerical continuation on the maximum value of the specific impulse value, $c_{\max}$, adding additional complexity. This method is referred to as the $c_{\max}$ method. While the $c_{\max}$ method (see Fig. 1) provides excellent initial convergence, it can face numerical difficulties during the final continuation iterations. To circumvent this convergence issue, $a_{\max}$ method is proposed for the final iterations. If a linear acceleration is considered in the cost functional, solutions lie entirely on a singular arc. To avoid singular arcs and to enforce optimal bang-off-bang acceleration profiles, a parameter, $a_{\max}$, is introduced to the problem formulation. This acceleration-based method, as is shown herein, is an elegant formulation to find optimal multi-impulse maneuvers. Furthermore, the continuation performed over the $a_{\max}$ value is observed to be much more well behaved than continuation on the thrust value. More specifically, large steps can be taken over the values of $a_{\max}$, resulting in fewer number of iterations to reach the near-impulsive solution.

As depicted in Fig. 1, the solution obtained from the acceleration-based method (which is near-optimal and has a fixed number of impulses, N) is used as an initial guess for a nonlinear-programming-based method that exploits a Lambert solver and the primer vector theory to determine the final N-impulse solution to a high precision. The proposed two-step algorithm, as is shown herein, builds a viable procedure to find many-impulse spacecraft maneuvers involving up to ≈50 orbital revolutions. To showcase the capability of the proposed methodology, a multirevolution rendezvous problem from a GTO to GEO and from GTO to L1 with a double-digit number of revolutions is presented. The method is capable of capturing even the low-magnitude impulses to find an optimal solution for a particular rendezvous problem with a fixed number of revolutions. For further verification purposes, a well-studied interplanetary maneuver from Earth to Mars and a more difficult benchmark rendezvous maneuver from Earth to asteroid Dionysus are also presented to demonstrate the efficacy of the algorithm. The local optimality of these trajectories is verified by showing that the resulting impulsive solutions satisfy Lawden's necessary conditions and match the optimal solutions in the literature.

The paper is organized as follows. Section II describes the mathematical formulation of the two proposed methods and explains the key components of the solution methodology. Section III first presents a brief discussion on the numerical setup and then the results of the considered examples with a detailed discussion are provided. Section IV concludes the paper.

II. Methodology

The trajectory optimization problems are formulated using the set of modified equinoctial elements (MEEs) [20] due to their amenability to convergence for multirevolution, low-thrust trajectories as demonstrated in literature [21,22]. Let m denote the spacecraft mass and let $\boldsymbol{x} = [p, f, g, h, k, l]^{\mathrm{T}}$ denote the vector associated with the MEEs. Let $\boldsymbol{a} = [a_r, a_t, a_n]^{\mathrm{T}}$ denote the acceleration vector owing to thrusting expressed in the LVLH (Local Vertical Local Horizontal) frame attached to the spacecraft. The time rate of change of MEEs can be written as

$$\dot{\boldsymbol{x}}(t) = \boldsymbol{A}(\boldsymbol{x}, t) + \mathbb{B}(\boldsymbol{x}, t)\boldsymbol{a}, \qquad \boldsymbol{a} = \frac{T}{m}\hat{\boldsymbol{\alpha}} \tag{1}$$

where $\boldsymbol{A} \in \mathbb{R}^{6\times 1}$ and $\mathbb{B} \in \mathbb{R}^{6\times 3}$ are defined in [22], T is the thrust magnitude, and $\hat{\boldsymbol{\alpha}}$ denotes the thrust unit steering vector (i.e., $\|\hat{\boldsymbol{\alpha}}\| = 1$). In the remainder of the paper, the explicit dependence of the A vector and $\mathbb{B}$ matrix to state, $\boldsymbol{x}$, are dropped for simplifying the algebraic relations. Under two-body dynamics assumptions, we formulate the transfer problems as time-fixed, rendezvous-type maneuvers. There are three major steps in the evaluation of the impulsive solutions outlined in Fig. 1 and explained in three subsections below.

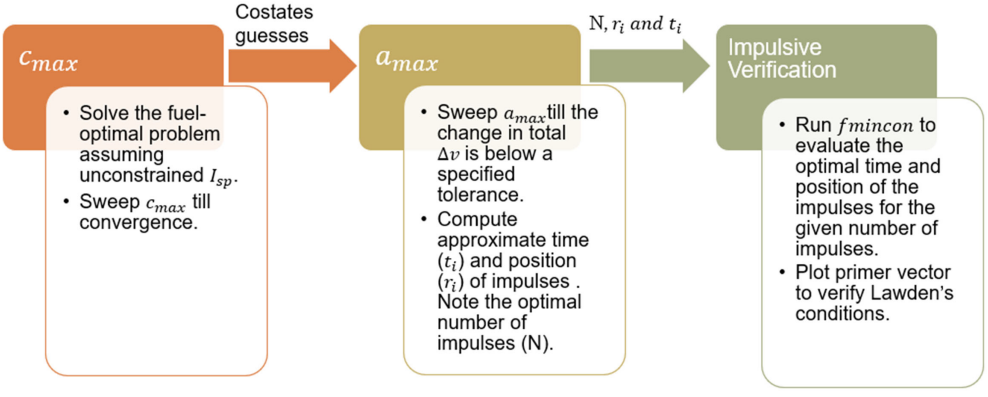

Fig. 1 Robust two-step optimization algorithm for generating multi-impulse trajectories.

A. Control Sweep Step

The foremost step in the algorithm is to obtain a near-impulsive solution that is accomplished using two methods applied individually or in succession: 1) the $c_{\max}$ method and 2) the $a_{\max}$ method with their details given in the following sections.

1. *The $c_{\max}$ Method*

This method is based on the operation of VIVT engines that are capable of providing continuous values for exhaust velocity and thrust. Though heretofore restricted to academic research, the concept of VIVT engines is a promising tool to obtain various initial optimal trajectories with different thrust modulations. Let I_{sp} denote the specific impulse value and let g_0 denote the Earth's gravitational acceleration at the equator. In VIVT engines, the exhaust velocity, $c = I_{\text{sp}} g_0$, is one of the control variables, which can be constrained to lie within an admissible range defined as $c \in [c_{\min}, c_{\max}]$ [23]. Here, $c_{\min}$ and $c_{\max}$ denote the minimum and maximum admissible exhaust velocity values, respectively. Therefore, for a VIVT engine, the thrust T and time differential equation for mass, $\dot{m}$, can be written as

$$T(t) = \frac{2\eta P}{c}\delta(t), \qquad \dot{m}(t) = -\frac{2\eta P}{c^2}\delta(t) \tag{2}$$

where $\delta(t) \in [0, 1]$ is engine throttle input. In Eq. (2), the thruster efficiency η is set to 1 (i.e., 100% thruster efficiency) and a constant power P_{use} is assumed to be available for thrusting, i.e., $P = P_{\text{use}}$. Both thrust and mass flow rate values are functions of c and the throttle input δ. Therefore, there are three control variables: throttle (δ), thrust unit steering vector ($\hat{\boldsymbol{\alpha}}$), and the exhaust velocity (c). With the state dynamics and control variables defined, the cost functional for minimizing fuel consumption is written as

$$\begin{aligned} \underset{\delta\in[0,1],\|\hat{\boldsymbol{\alpha}}\|=1,c\in[c_{\min},c_{\max}]}{\text{Minimize}} \quad & J = \int_{t_0}^{t_f} \frac{2\eta P}{c^2}\delta(t)\,\mathrm{d}t, \\ \text{subject to:} \quad & \\ & \text{Eqs. (1) \& (2)}, \boldsymbol{x}(t_f) - \tilde{\boldsymbol{x}}_d = \boldsymbol{0}, P = P_{\text{use}}, \\ & \boldsymbol{x}(t_0) = \boldsymbol{x}_0, m(t_0) = m_0, \eta = 1 \end{aligned} \tag{3}$$

where t_0 is the initial time; $\boldsymbol{x_0}$ and m_0 are the MEEs and mass of the spacecraft at the initial time, respectively; t_f is the final time; $\Delta t = t_f - t_0$ is the time of flight; P_{use} is the power available for thrusting set by the user; and $\tilde{\boldsymbol{x}}_d$ is the desired MEEs at the final time. The (optimal control) Hamiltonian associated with the defined cost functional and state dynamics is

$$H = \frac{2\eta P}{c^2}\delta + \boldsymbol{\lambda}^{\top}\left(\boldsymbol{A} + \frac{T}{m}\mathbb{B}\delta\hat{\boldsymbol{\alpha}}\right) - \lambda_m \frac{2\eta P}{c^2}\delta \tag{4}$$

where $\boldsymbol{\lambda} = [\lambda_p, \lambda_f, \lambda_g, \lambda_h, \lambda_k, \lambda_l]^{\top}$ is the costate vector associated with the MEEs and λ_m is the costate associated with mass. Due to the bilinear appearance of $\hat{\boldsymbol{\alpha}}$ and δ in the Hamiltonian, Pontryagin's minimum principle (PMP) is used to find the optimal control direction, which is aligned along the Lawden's primer vector $\boldsymbol{p} = -\mathbb{B}^{\top}\boldsymbol{\lambda}$ defined as

$$\hat{\boldsymbol{\alpha}}^* = \frac{\boldsymbol{p}}{\|\boldsymbol{p}\|} = -\frac{\mathbb{B}^{\top}\boldsymbol{\lambda}}{\|\mathbb{B}^{\top}\boldsymbol{\lambda}\|} \tag{5}$$

According to the PMP, the throttle input δ has to be selected such the Hamiltonian is minimized along an extremal solution

$$\delta^* = \arg\min_{\delta\in[0,1]} H(\boldsymbol{x}^*(t), m^*(t), \delta(t), \boldsymbol{\lambda}^*(t), \lambda_m^*(t)) \tag{6}$$

and the thrust switching function that governs the optimal throttle (δ) "on" or "off" modes can be defined as

$$\delta^* = \begin{cases} 1; & \text{for } SF > 0,\ \forall\ c \in [c_{\min}, c_{\max}], \\ 0; & \text{for } SF \le 0,\ \forall\ c \in [c_{\min}, c_{\max}] \end{cases} \tag{7}$$

$$SF = \frac{c_{\max}\|\mathbb{B}^{\top}\boldsymbol{\lambda}\|}{m} + \lambda_m - 1 \tag{8}$$

Singular control arcs may occur when the switching function remains zero over a finite time interval, but singular arcs are not treated in this work since they rarely occur in space flights. The discontinuous structure of the theoretically extremal control, δ^* given in Eq. (7), is made smooth, yet approximated to a high precision, using the hyperbolic tangent smoothing (HTS) method [24] as

$$\delta^* \approx \delta(SF, \rho_b) = 0.5\left[1 + \tanh\left(\frac{SF}{\rho_b}\right)\right] \tag{9}$$

where ρ_b is a smoothing parameter that controls the sharpness of the switch of the optimal bang-off-bang throttle input. The time rate of change of costates can be evaluated by Euler–Lagrange equations as

$$\dot{\boldsymbol{\lambda}} = -\left[\frac{\partial H}{\partial \boldsymbol{x}}\right]^{\top}, \qquad \dot{\lambda}_m = -\frac{\partial H}{\partial m} \tag{10}$$

Optimal values of specific impulse can be characterized using the strong form of optimality, $\partial H/\partial c = 0$, giving an expression for c_{opt} [25] as

$$c_{\text{opt}} = \frac{2(1-\lambda_m)m}{\|\mathbb{B}^{\top}\boldsymbol{\lambda}\|} \tag{11}$$

Using Eq. (11) along with the admissible bounding constraint that $c_{\text{opt}} \le c_{\max}$, the effective optimal exhaust velocity ($\tilde{c}$) becomes

$$\tilde{c} = \begin{cases} c_{\max}, & \text{if } c_{\text{opt}} \ge c_{\max}, \\ c_{\text{opt}}, & \text{if } c_{\text{opt}} \le c_{\max} \end{cases} \tag{12}$$

To accommodate the above inequality condition imposed on the selection of $\chi_{c_{\max}}$, a smooth structure of $\tilde{c}$ is obtained by the use of an activation function such as

$$\tilde{c} = \chi_{c_{\max}} c_{\max} + (1 - \chi_{c_{\max}}) c_{\text{opt}} \tag{13}$$

where the activation function is constructed using the HTS method as

$$\chi_{c_{\max}} = 0.5\left[1 - \tanh\left(\frac{c_{\max} - c_{\text{opt}}}{\rho_c}\right)\right] \tag{14}$$

where ρ_c is a smoothing parameter to control the enforcement of the $c_{\text{opt}} \le c_{\max}$ constraint.

According to PMP, the Hamiltonian should be minimized over all the set of admissible controls. Therefore, $c_{\max}$ is used to evaluate the SF in Eq. (8) to allow the VIVT engine to be ON, if at least one admissible value of c exists that makes the power switching function SF positive [26]. In case of the unconstrained formulation, the inequality given in Eq. (14) is not used since $c_{\max}$ is set to a high enough value such that $\tilde{c} = c_{\text{opt}}$ is always followed. This also removes the presence of any throttle discontinuity as PMP dictates the thruster to be always 'on' in this case. Additionally, we have the mass costates terminal boundary condition $\lambda_m(t_f) = 0$ since final spacecraft mass, $m(t_f)$, is free. Let $\tilde{x}_d$ denote the desired/target MEEs. Thus, the set of final boundary conditions can be defined as

$$\boldsymbol{\Gamma} = [(\boldsymbol{x}(t_f) - \tilde{\boldsymbol{x}}_d)^{\top}, \lambda_m(t_f)]^{\top} = \boldsymbol{0} \tag{15}$$

The optimal control expressions along with the state and costate and boundary conditions form a two-point boundary-value problem (TPBVP). More specifically, state dynamics, Eqs. (1) and (2);

costate dynamics, Eq. (10); and extremal control expressions, Eqs. (5), (9), and (13), along with the set of final constraints, Eq. (15), define the TPBVP associated with the $c_{\max}$ method. The TPBVP can be formulated as a nonlinear root-finding problem that can be written as

$$\boldsymbol{\Gamma}(\boldsymbol{\eta}(t_0);\boldsymbol{\Theta}) = [(\boldsymbol{x}(t_f) - \tilde{\boldsymbol{x}}_d)^\top, \lambda_m(t_f)]^\top = \boldsymbol{0} \tag{16}$$

where $\boldsymbol{\eta}(t_0) = [\boldsymbol{\lambda}(t_0)^\top, \lambda_m(t_0)]^\top$ denotes the unknown costates at the initial time and $\boldsymbol{\Theta} = [\rho_b, \rho_c, c_{\max}]$ denotes the vector of continuation parameters of the resulting TPBVPs. Note that, for solving each TPBVP, Θ is fixed, but the continuation parameters will be modified using a standard continuation method to guide the solution of the resulting TPBVPs to the solution of the TPBVP associated with a near-impulsive solution. For the unconstrained case in which the constraint [given in Eq. (14)] is removed from the problem formulation, $\boldsymbol{\Theta} = c_{\max}$. Upon obtaining an optimal solution for the unconstrained version, a continuation procedure is initiated (with $\boldsymbol{\Theta} = [\rho_b, \rho_c, c_{\max}]$) in which the value of $c_{\max}$ can be swept from a high value (ideal engine) to a low value (chemical engine) to ultimately obtain a near-impulsive solution.

Typically, the introduction of the constraint ($c_{\min} \le c \le c_{\max}$) in the exhaust velocity is considered to represent the performance constraints of a realistic engine. But even with a propulsion model featuring unconstrained and unrealistically high-I_{sp} engine, the VIVT propulsion modeling produces excellent initial optimized trajectories with relatively arbitrary boundary conditions.

There are two major advantages of using the unconstrained VIVT solution to kick-start the optimization:

1) The fuel-optimal solution of the unconstrained version of the VIVT modeling uses the optimal I_{sp} at all times [see Eq. (11)], resulting in a continuous thrust trajectory ($\delta = 1$) with no control discontinuities. Hence, it facilitates numerical convergence.

2) The only control variable affecting the thrust and mass flow rate [Eq. (2)] is c_{opt}, which is a function of the instantaneous mass [see Eq. (11)]. This allows flexibility in choosing arbitrary initial mass and time of flight. The exhaust velocity values using arbitrary mass and power values despite being unrealistic aid in better selection of these parameters in consecutive steps of the solution procedure (see Fig. 1).

Alternatively, many previous works have established an objective function where the integral of acceleration squared is minimized [4]. This also leads to a continuous trajectory similar to the unconstrained $c_{\max}$ method described above. The authors have chosen to use the current method over the traditional one due to the ease of convergence displayed by $c_{\max}$ over the pure acceleration squared method (A^2 method). The reason partly lies in the dependence of the control magnitude on the selection of Lagrange multipliers in the case of the A^2 method. This leads to an increase in sensitivity of the trajectory toward the magnitude of the iterated Lagrange multipliers. In the case of unconstrained $c_{\max}$, the direction and the magnitude of the thrust vector are not as coupled, which increases the domain of convergence of the nonlinear root-solving problem.

In summary, the original difficult-to-solve optimal control problem (OCP) associated with the multi-impulse trajectories is embedded in a three-parameter (i.e., ρ_b, ρ_c, and $c_{\max}$) family of neighboring TPBVPs [see Eq. (16)]. When $c_{\max}$ value is low, the solution is forced to have coast arcs and as the $c_{\max}$ value is lowered further, it forces the thrust arcs to be very narrow more in line with an impulsive solution. Therefore, a standard numerical continuation is used to solve the TPBVPs in which the converged costates of the previous iteration are used as an initial guess to improve convergence of the subsequent iterations. In practice, we have found that large steps (only 3–4 iterations) in the $c_{\max}$ value are needed to obtain a near-impulsive solution for the simple (first two of the four representative) maneuvers considered in this paper. Detailed information on the implementation and the numerical values are given in Sec. III.

One primary difficulty encountered in the $c_{\max}$ method is the possibility of getting near-zero mass values for a randomly selected initial guess for costates especially when a low $c_{\max}$ value is set (typically during the last iterations). Note that lower $c_{\max}$ values are ideal to recover impulsive thrust arcs [i.e., high thrust in Eq. (2)]. Therefore, a second method is proposed, which can be used individually in some cases or in continuation to the $c_{\max}$ method to circumvent this problem.

2. *The $a_{\max}$ Method*

Impulsive solutions contain velocity-level information. A pure acceleration-based formulation is proposed that removes the dependency of the problem formulation to mass, specific impulse, and thrust value. The removal of these parameters makes the problem substantially easier given that the mass state and its associated costate (i.e., $\dot{m}$ and $\dot{\lambda}_m$) are removed from the formulation of the OCP. A fixed-time, rendezvous-type, minimum-Δv trajectory optimization problem is considered with a cost functional defined in Lagrange form as

$$\underset{\boldsymbol{a}\in\boldsymbol{\Omega}}{\text{minimize}}\ J = \int_{t_0}^{t_f} \|\boldsymbol{a}\|\,\mathrm{d}t \tag{17}$$

where t_0 and t_f are the initial and final times, respectively, and $\boldsymbol{\Omega}$ denotes the set of admissible acceleration vectors. To enforce optimal bang-off-bang acceleration profiles, a bound on maximum acceleration $a_{\max}$ is introduced to the problem formulation. In this formulation, the thruster acceleration is rewritten as $\boldsymbol{a} = a_{\max}\hat{\boldsymbol{\alpha}}\delta$, where $a_{\max}$ is used to embed the original OCP into a family of neighboring OCPs. Therefore, the modified cost functional for minimizing acceleration can be stated as

$$\begin{aligned}&\text{Minimize}\quad J = \int_{t_0}^{t_f} \delta a_{\max}\,\mathrm{d}t,\\ &\text{subject to:}\\ &\qquad \text{Eq. (1)}, \boldsymbol{x}(t_f) - \tilde{\boldsymbol{x}}_d = \boldsymbol{0}, \boldsymbol{x}(t_0) = \boldsymbol{x}_0, a_{\max}\text{: user defined}\end{aligned} \tag{18}$$

Upon writing the Hamiltonian as

$$H = \delta a_{\max} + \boldsymbol{\lambda}^\top[\boldsymbol{A} + a_{\max}\mathbb{B}\delta\hat{\boldsymbol{\alpha}}] \tag{19}$$

the optimal thrust direction is still governed by $\hat{\boldsymbol{\alpha}}^*$ [see Eq. (5)]. The costate dynamics are derived using Euler–Lagrange equation as

$$\dot{\boldsymbol{\lambda}} = -\left[\frac{\partial H}{\partial \boldsymbol{x}}\right]^T \tag{20}$$

Employing the PMP to determine δ, the smooth throttle input can be written as

$$\delta^* \approx \delta(SF, \rho_b) = 0.5\left[1 + \tanh\left(\frac{SF}{\rho_b}\right)\right] \tag{21}$$

where $SF = \|\mathbb{B}^\top\boldsymbol{\lambda}\| - 1$. The TPBVP associated with the cost functional, Eq. (18); the state dynamics, Eq. (1) with $\boldsymbol{a} = a_{\max}\,\hat{\boldsymbol{\alpha}}\delta$; the costates given in Eq. (20); and the control inputs given in Eqs. (5) and (21) can be written as a nonlinear root-finding problem given in Eq. (22):

$$\boldsymbol{\Gamma}(\boldsymbol{\eta}(t_0);\boldsymbol{\Theta}) = \boldsymbol{x}_{\text{MEE}}(t_f) - \tilde{\boldsymbol{x}}_d = \boldsymbol{0} \tag{22}$$

where $\boldsymbol{\Theta} = [\rho_b, a_{\max}]$ denotes the continuation parameters of the resulting TPBVPs. Thus, a two-parameter family of neighboring OCPs is formed, with a reduced number of equations, simpler form of the switching function, no dependence on engine parameters, less number of constraints, and only two continuation parameters. In Eq. (22), there is a total of six scalar final constraints.

There are notable advantages of the $a_{\max}$ method:

1) The number of differential equations is reduced to 12 with mass removed.

2) The selection of exhaust velocity as a control variable is not required.

3) Large steps in $a_{\max}$ can be taken without getting trapped in intermediate valleys, which could otherwise make convergence difficult [12].

The value of $a_{\max}$ is swept from a relatively low to a high value until the thrust acceleration arcs become narrow enough to give a good approximation of an impulsive solution. The numerical continuation procedure for solving the resulting TPBVPs is identical to the $c_{\max}$ method. However, the set of continuation parameters consists of only two parameters, i.e., ρ_b and $a_{\max}$. The former is used to enforce bang-off-bang acceleration profile, whereas the latter is used to achieve minimum-ΔV maneuvers. We would like to emphasize that both $c_{\max}$ and $a_{\max}$ methods lead to near-optimal solutions for simple problems (e.g., the first two problems that we considered in this paper). It is only for difficult problems that a two-step procedure is recommended, per Fig. 1.

B. Primer Vector Theory Step

In this subsection, a straightforward procedure of extracting the results from the control sweep (CS) step is described, which supplies a very good initial guess to obtain the exact impulsive solution that satisfies Lawden's necessary conditions.

1. *Impulses Extraction*

Each narrow thrust arc obtained from the previous step is treated as an individual impulse. The midpoint of each individual short finite burn arc is taken as the point of impulse, and the time and position for each of these midpoints are noted. The direction of the primer vector at this midpoint approximates the direction of the impulse, and the integral of acceleration over the short burn arcs approximates the velocity impulse magnitude.

The quality of this starting estimate warrants the exactness of the number of impulses, which is not required to be introduced as a design variable. The only design variables that are required to be iterated upon are the positions and times of the interior as well as departure and arrival impulses (if the problem happens to have impulses at the boundaries). This approximate optimal impulsive solution can feature both *late departure* or *early arrival* but does not allow an increase in the time of flight [12].

C. Impulsive Verification

The time of flight (and the trajectory as a consequence) is divided into time segments featuring an impulse at each end. On each intervening coast arc, two-body dynamics are assumed and the transfer arc is computed using a Lambert solver. Utilizing excellent estimates of the times, directions, and magnitudes of the velocity impulses from the previous step, a nonlinear programming (NLP) solver, MATLAB's `fmincon`, is used to minimize the cost defined as [12]

$$\text{Minimize } J = \Delta v_{total} = \sum_{k=1}^{N} \Delta v_k \tag{23}$$

where Δv_k is the magnitude of the kth impulse vector and N denotes the total number of impulses. The design variables for `fmincon` are the time of flight of each segment (Δt_k) and the position of impulses ($\boldsymbol{r}_k$) with appropriate bounds set on each. Upon convergence of `fmincon`, the primer vector $\boldsymbol{p}$ is plotted using the procedure outlined in [Sec. II.B] and [27]. The resulting primer vector of the optimized solution is verified against Lawden's necessary conditions. Violation of these necessary conditions has been used to determine suboptimality of impulsive solutions [4,28] and hence is used as a prerequisite validation check for an extremal impulsive solution.

III. Numerical Simulation and Results

To solve the resulting TPBVPs, MATLAB solver `fsolve` is used with tolerances on the search step-size, TolX and TolFun, which relates to both the size of the latest change in sum of squares of the residuals and the relative norm of the gradient of this sum of squares, respectively. The relative norm of the gradient is used to determine the stopping condition. The maximum number of iterations and function evaluations are also set as given in Table 1. The number of iterations and function evaluations are chosen by experience, to avoid spending extra time in solving infeasible cases. The solver is set to use interior-point algorithm, and the Jacobian is set to be "on" if analytical sensitivities are provided to the solver.

Table 1 Settings used for MATLAB's `fsolve` and `fmincon` functions

Parameter	`fsolve`	`fmincon`
Tolfun	1.0×10^{-10}	1.0×10^{-10}
TolX	1.0×10^{-14}	1.0×10^{-14}
Maximum function evaluations	500	1000
Maximum iterations	300	300
Jacobian	ON	OFF

The most significant difficulty encountered in this work is the sensitivity of the resulting TPBVPs with respect to initial costates in the case of many-revolution trajectories. To circumvent this problem, a two-step process is defined, where the $c_{\max}$ method is quick to converge for the initial iterations but its convergence can degrade in the later iterations when the $c_{\max}$ value is set quite low to recover near-impulsive solutions. Therefore, for an arbitrary intermediate value of $c_{\max}$, the costates and the associated acceleration value from the solution are used to feed the $a_{\max}$ method to get the final near-optimal, near-impulsive solution.

In most problems, MATLAB's built-in finite difference method is used to evaluate the Jacobian to aid Newton's gradient-based solvers. For this work, analytical sensitivities are computed at each time to feed to the solver without which convergence becomes difficult as the dimensionality becomes large. MATLAB's `fsolve` only accepts first derivative. To calculate the derivate information of the residual vector of the resulting TPBVPs with respect to the decision variables (i.e., the initial value of the costates), one can form the differential equations of the state transition matrix. The matrix differential equation is then converted into a vector form, and appended to the set of state–costate differential equations. The implementation details are given in [29,30]. Four example problems are presented: The heliocentric phase of two interplanetary maneuvers 1) from Earth to Mars (E2M), 2) from Earth to asteroid Dionysus (E2D), 3) a geocentric maneuver from a geostationary transfer orbit (GTO) to GEO (G2G), and 4) a GTO to a circular orbit with a radius equal to the distance from the Earth to the L1 point of the Earth–moon system (GTO2L1). Canonical normalization [31] is used for the equations of motion with different characteristic values as per the transfer. For the E2M and E2D problems, $\mu = 132{,}712{,}440{,}018$ km^3/s^2 and DU = AU = 149.6×10^6 km, while for the G2G problem, $\mu = 398{,}600$ km^3/s^2 and DU = 6378 km (Earth's radius). For the GTO2L1 problem, $\mu = 398{,}600$ km^3/s^2 and DU = 42,164 km. In the "Impulsive verification" step, the initial guesses for the position vector and time of impulses are fed into MATLAB's (2019b version) `fmincon` with its settings listed in Table 1. Analytical sensitivities are not provided to this solver.

A. Earth to Mars

To demonstrate the utility of the $c_{\max}$ method, a simple rendezvous example from Earth to Mars is solved with the following MEE boundary conditions: $p(t_0) = 1.0005515$ (AU), $f(t_0) = -0.0029454$, $g(t_0) = 0.0162404$, $h(t_0) = 1.0847571 \times 10^{-5}$, $k(t_0) = 8.446336 \times 10^{-7}$, and $L(t_0) = 7.4484263$. For the target state, $p_d = 1.5103483$ (AU), $f_d = 0.0854214$, $g_d = -0.0378510$, $h_d = 0.0104734$, $k_d = 0.01228042$, and $L_d = 17.4484552$.

As explained in Sec. II, first a solution with unconstrained VIVT formulation is obtained, which exhibits a continuous thrust profile as shown in Fig. 2. Here, the increase in the values of I_{sp}, causing a sudden drop in the thrust value, compensates for the regions where the optimality would have warranted a coast arc. As lowering of $c_{\max}$ parameter by use of constrained VIVT formulation is conducted,

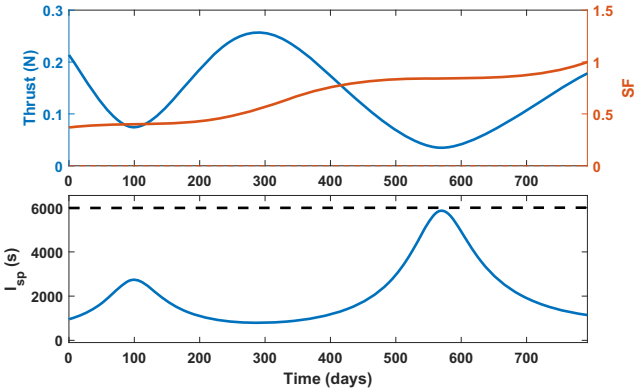

Fig. 2 E2M problem: thrust profile and I_{sp} vs time for the unconstrained VIVT formulation.

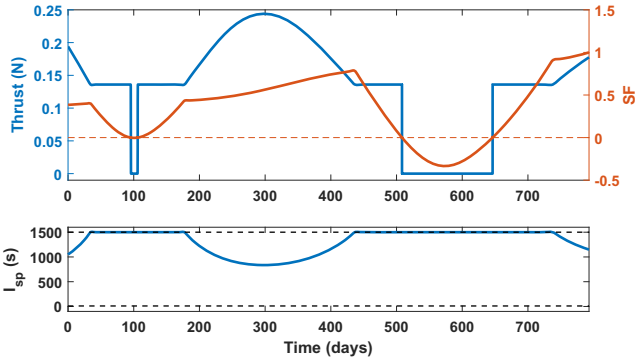

Fig. 3 E2M problem: thrust profile and I_{sp} with $I_{sp,max} = 1500$ s.

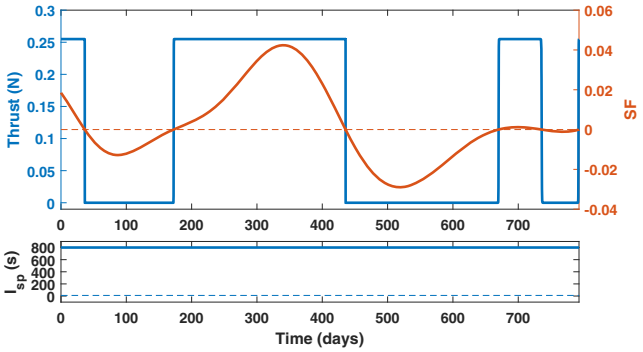

Fig. 4 E2M problem: thrust profile and I_{sp} with $I_{sp,max} = 800$ s.

coast arcs start to appear. Two of these iterations are shown in Figs. 3 and 4, which are plotted for $\rho_b = \rho_c = 1 \times 10^{-5}$.

Unlike the $I_{sp,max} = 1500$ s case (see Fig. 3), where c_{opt} is still lesser than the set c_{max} during certain time intervals, the exhaust velocity is completely saturated at c_{max} when $I_{sp,max} = 800$ s as shown in Fig. 4. Any lowering in c_{max} from this point is equivalent to a thrust continuation process. The final near-impulsive solution depicted in Fig. 5 corresponds to a $\Delta v_{total} = 5.62$ km/s. The details on the time and magnitude of impulses for this near-optimal, near-impulsive solution are given in Table 2.

The solution obtained from the above procedure in terms of number of impulses, position, and time of impulses is fed into the nonlinear solver (primer vector theory [PVT] step described in Sec. II) as an initial guess to converge to the exact impulsive maneuver. The optimal primer vector obtained from the converged solution of `fmincon` (see Fig. 5) satisfies Lawden's conditions. Notice that the obtained primer vector profile matches the switching function obtained from the CS step.

The total ΔV (Δv_{total}) from this PVT step is 5.6109 km/s with some small variation in the departure time from the CS step solution. The complete comparison of the optimal impulsive solution obtained from CS and PVT is given in Table 2. The optimal impulsive trajectory obtained from PVT is given in Fig. 6. The optimal impulsive solution matches the known solution in the literature [12].

B. Earth to Dionysus

A difficult rendezvous problem with multiple orbital revolutions around the sun is solved in this section using the a_{max} method. Though the E2D problem can be solved using both c_{max} and a_{max} methods, the latter is chosen to provide the reader clarity over both the methods. The E2D problem is another standard problem in its own right having been studied in great detail in [12] with different ΔV solutions and time of flight associated with different numbers of revolutions. Impulsive solution associated with the number of orbital revolutions of 5,

Table 2 Comparison of the E2M impulsive solutions

Parameter	Value
c_{max} solution	
Δv_{total} (km/s)	5.62
Time of impulses (days)	[1.9922, 360.6356, 715.29368]
Magnitude of impulses (km/s)	[1.425, 1.928, 2.268]
PVT solution	
Δv_{total} (km/s)	5.6109
Time of impulses (days)	[0.0198817, 360.6553, 713.7880
Magnitude of impulses (km/s)	[1.439, 1.891, 2.281]

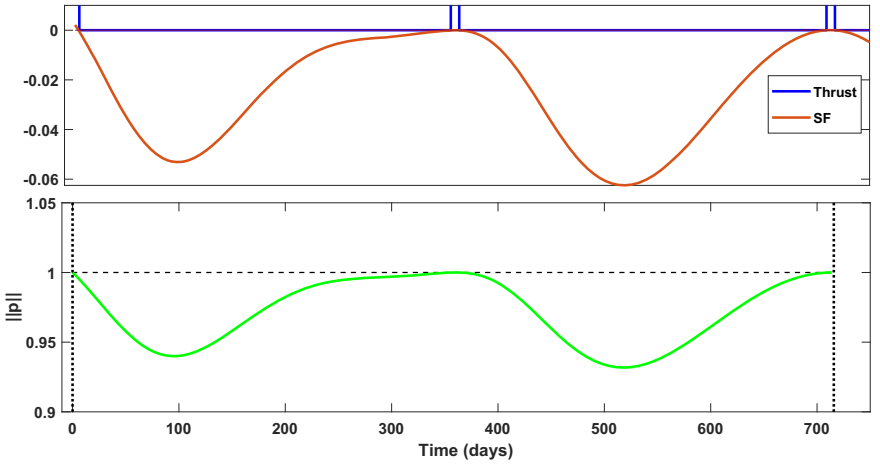

Fig. 5 E2M problem: thrust and switching function of approximate impulsive solution (top) and norm of the primer vector for the optimal impulsive solution (bottom).

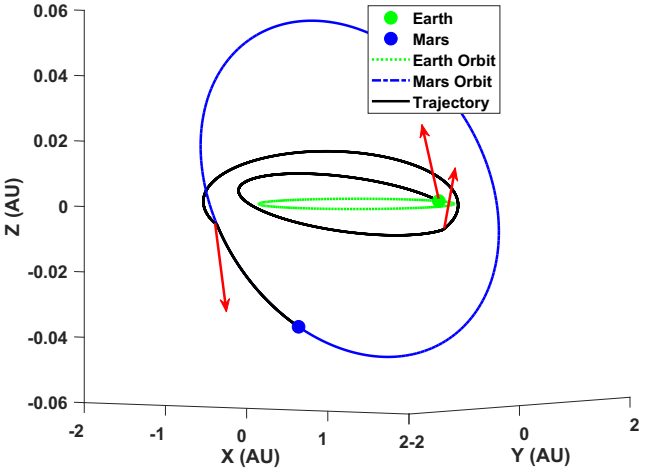

Fig. 6 E2M problem: three-impulse, minimum-ΔV trajectory. Red arrows denote impulses.

$N_{\text{rev}} = 5$, is solved in this work with a fixed time of flight of 3534 days and boundary conditions (in MEEs) defined as $p(t_0) = 0.9996943$ (AU), $f(t_0) = -0.00376679$, $g(t_0) = 0.01628689$, $h(t_0) = -7.7020614 \times 10^{-6}$, $k(t_0) = 6.1881685 \times 10^{-7}$, and $L(t_0) = 14.1618925$. For the target state, $p_d = 1.5536970$ (AU), $f_d = -0.5199481$, $g_d = 0.0161831$, $h_d = 0.0104734$, $k_d = 0.1181395$, and $L_d = 46.3302403$.

Starting from a relatively low value of $a_{\max}$, a continuation procedure of increasing $a_{\max}$ is conducted until the change in Δv_{total} is below a prescribed threshold (e.g., 1% relative to its previous value) as shown in Fig. 7. For each value of $a_{\max}$ in the continuation step, the continuation parameter ρ_b [defined in Eq. (21)] is decreased till 1.0×10^{-3} to capture thrust acceleration arcs with an acceptable accuracy for the next $a_{\max}$ iteration. For $\rho_b = 1.0 \times 10^{-3}$, all the thrust arcs might not be sharp, but to save computational effort, the continuation in ρ_b could be stopped as it still provided enough information for the next iteration. The final result corresponding to $a_{\max} = 1.0 \times 10^{-3}$ m/s^2 is shown in Fig. 8. Figure 9 shows the time history of the primer vector magnitude associated with the impulsive solution that displays satisfaction of Lawden's necessary conditions. Since all impulses are intermediate impulses, the derivative of the norm of the primer vector is zero at the time of impulses and $\|\boldsymbol{p}\| = 1$ [27]. Figure 10 shows the impulsive trajectory, where the first five impulses are applied at the perihelion passages of the intermediate elliptical orbits and the last impulse is applied at the intersection of the last elliptical orbit with the orbit of the asteroid Dionysus.

The importance of impulsive maneuvers for reachability analysis can be observed in the significant reduction in the time of flight with ideal impulsive solutions, even when the original continuous thrust acceleration was applied along the trajectory. In fact, the effective time of flight can be considered to be from the first impulse till the last impulse and the early and late coast arcs are redundant. The shift in the time of flight can be observed very clearly if $a_{\max}$ (opposed to thrust sweeps in [12]) is swept to generate a surface. This switching function, for minimized-acceleration-integral switching surface shown in Fig. 11, is quite similar to the minimum-fuel switching surface (by sweeping $T_{\max}$ value) as shown in Fig. 12. Notice that there are some different times for the zero crossing of the switching function near the peaks of the switching surfaces when the control variable ($a_{\max}$ or $T_{\max}$) is relatively small. The two switching surfaces are almost identical for the impulsive limits (see Fig. 13),

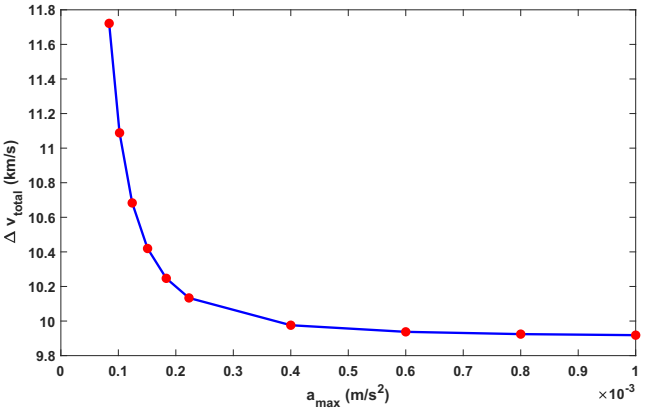

Fig. 7 E2D problem: continuation trend for Δv_{total} vs $a_{\max}$.

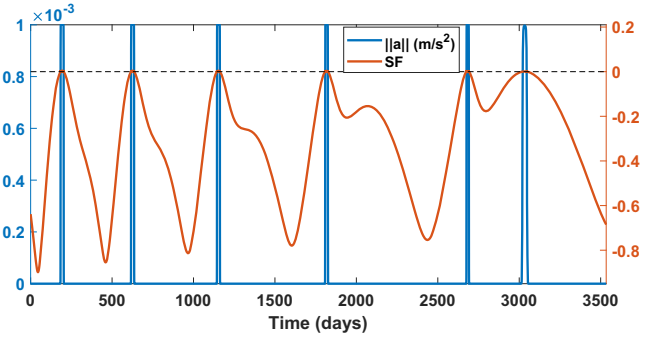

Fig. 8 E2D problem: thrust and switching function vs time for $a_{\max} = 1.0 \times 10^{-3}$ m/s^2.

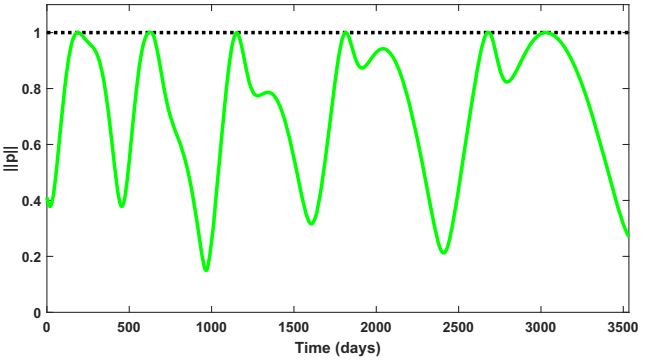

Fig. 9 E2D problem: primer vector magnitude vs time with $N_{\text{rev}} = 5$.

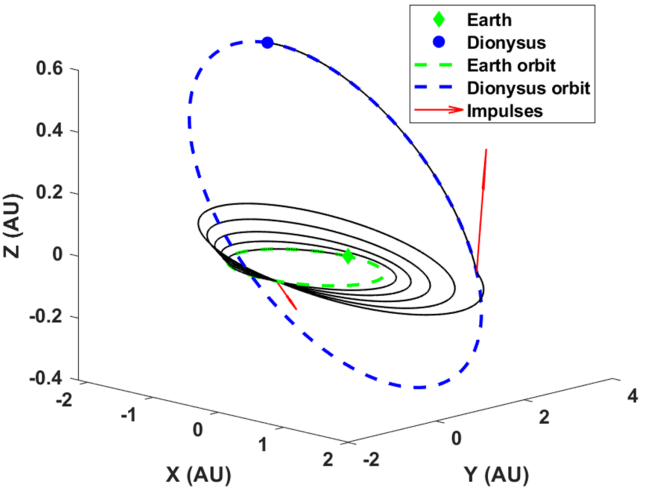

Fig. 10 E2D problem: six-impulse, minimum-ΔV trajectory.

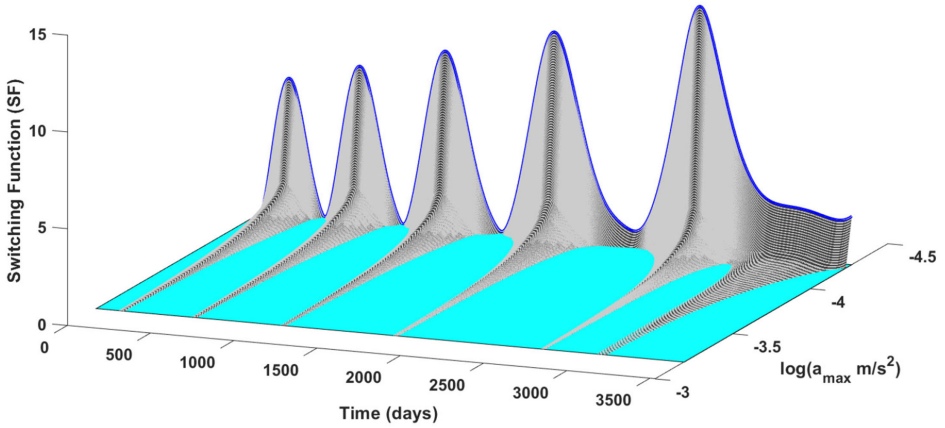

Fig. 11 E2D problem: maximum acceleration sweep switching surface.

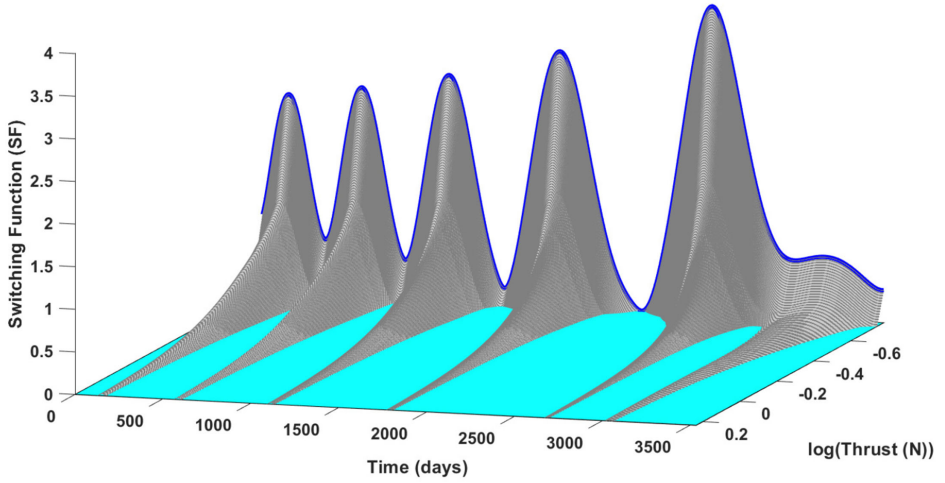

Fig. 12 E2D problem: maximum thrust sweep switching surface.

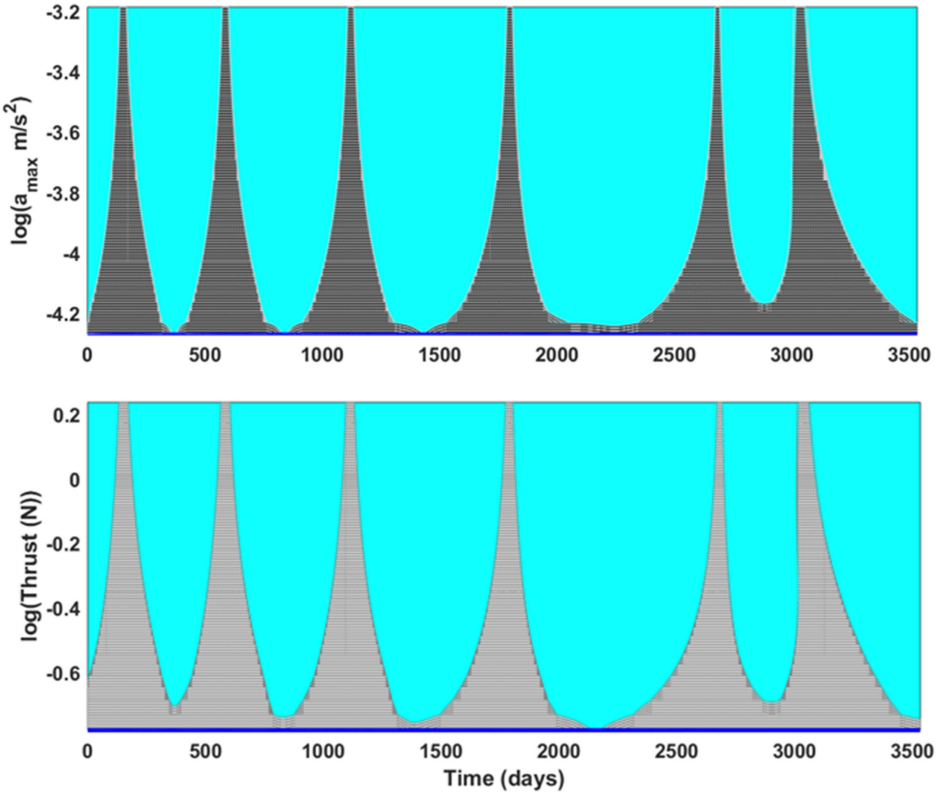

Fig. 13 $S = 0$ contours of the acceleration- and thrust-based switching surfaces in the top and bottom plots, respectively.

Table 3 Comparison of the minimum-ΔV solutions for the E2D problem

$a_{\max}$ solution ($\Delta v_{\text{total}} = 9.9183$ km/s)		Impulsive solution ($\Delta v_{\text{total}} = 9.90742$ km/s)	
Time (days)	ΔV (km/s)	Time (days)	ΔV (km/s)
193.377	1.6488	193.246	1.722
626.049	1.6097	629.608	1.4666
1153.166	1.5501	1152.099	1.6231
1816.915	1.4525	1816.969	1.44027
2683.504	1.2759	2683.731	1.2689
3033.693	2.3811	3032.192	2.3858

corroborating the fact that both methods approach the impulsive maneuver and the impulsive maneuver is independent of the thrust performance and mass of the engine. This thruster independence is harnessed especially in the acceleration-based switching surfaces, which provides different manifolds of trajectories possible for the fixed boundary conditions and an upper limit set on the time of flight and acceleration values ($a_{\max}$). In fact, the optimization process underlying Fig. 11 is simply the finite acceleration, finite pulse duration generalization of the impulsive minimum-Δv optimization. This also provides an improved reachability analysis, where the minimum acceleration value pertaining to the continuous control solution for a particular $a_{\max}$ value aids in engine selection. Table 3 summarizes the results, and it shows that the obtained impulsive solution is identical to the known solution reported in the literature [12].

C. GTO to GEO

In comparison to the last two problems, a more difficult multi-revolution geo-centric problem is considered. The maneuver involves 21 revolutions around the Earth, with MEE boundary conditions being

$$\boldsymbol{x}_0 = [1.8283296\ (\text{DU}), 0.725, 0, 0.06116262, 0, 0]^{\mathsf{T}},$$

$$\tilde{\boldsymbol{x}}_d = [6.66110065\ (\text{DU}), 0,0,0,0,135.0884841]^{\mathsf{T}}$$

The equivalent classical orbital elements $(a, \text{ecc}, \text{inc}, \omega, \Omega, \nu)$ defining this transfer are $\boldsymbol{\Psi}_o = [3.832467\ \text{DU}, 0.725, 7\ \text{deg.}, 0, 0, 0]$ and $\boldsymbol{\Psi}_f = [6.66110065\ \text{DU}, 0, 0\ \text{deg.}, 0, 0, \pi]$, where a is the semimajor axis, ecc denotes eccentricity, inc is the inclination, ω is argument of perigee, Ω is right ascension of the ascending node, and ν is the true anomaly. The parameters used are $P_{\text{use}} = 500$ W, and $m_0 = 250$ kg, $\Delta t = 16$ days, and the number of revolutions is set to be 21. The solution

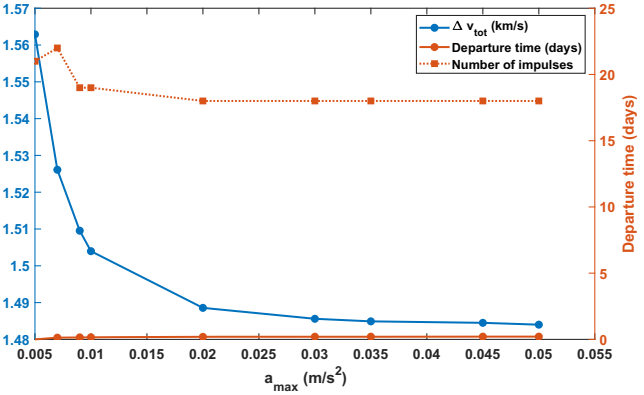

Fig. 15 G2G problem: ΔV, departure time since the initial epoch, and the number of impulses are plotted against the sweeping parameter $a_{\max}$.

to the unconstrained $c_{\max}$ method displays a continuous thrust profile as depicted in Fig. 14 with a $\Delta v_{\text{total}} \approx 2$ km/s and the largest value of I_{sp} recorded as 2202 s. After solving the unconstrained $c_{\max}$ problem, the solution is fed to the $a_{\max}$ method sweeping $a_{\max} \in [5 \times 10^{-3}, 5 \times 10^{-2}]$ m/s^2 as is shown in Fig. 15.

The solution shown here corresponds to a total number of 18 impulses amounting to $\Delta v_{\text{total}} \approx 1.484$ km/s for $a_{\max} = 3.5 \times 10^{-2}$ m/s^2 as shown in the Fig. 16. The resulting acceleration profile

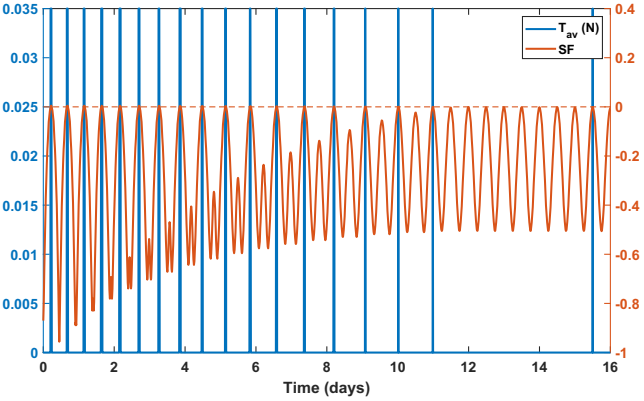

Fig. 16 G2G problem: near-optimal impulsive solution with $a_{\max} = 3.5 \times 10^{-2}$ m/s^2.

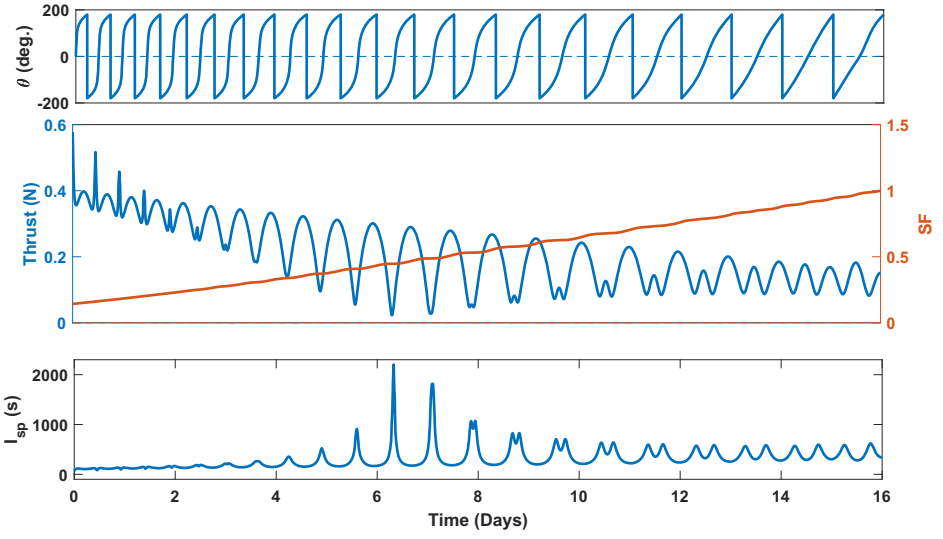

Fig. 14 G2G problem: optimal thrust and switching function profiles for unconstrained I_{sp} using the $c_{\max}$ method.

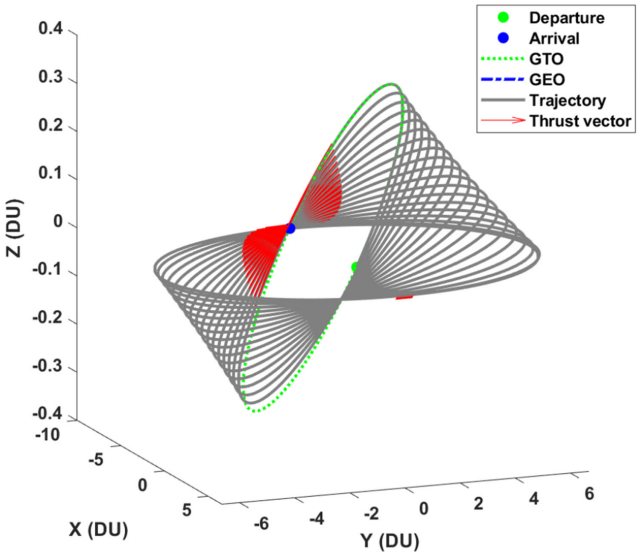

Fig. 17 G2G problem: near-optimal trajectory for $a_{\max} = 3.5 \times 10^{-2}$ m/s^2.

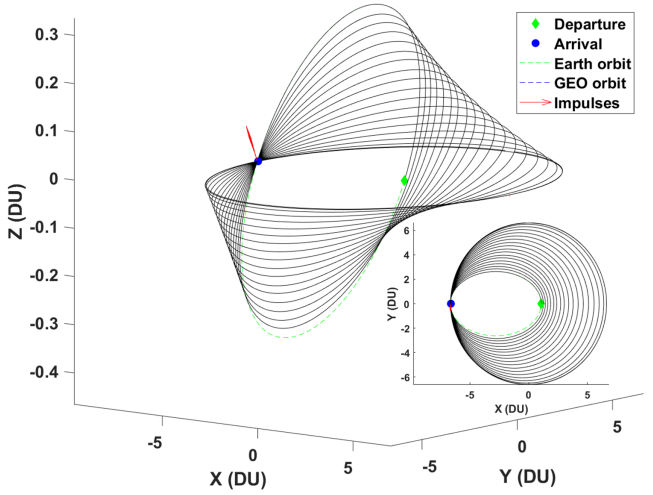

Fig. 18 G2G problem: impulsive trajectory.

displays a late departure and an early arrival kind of profile, as shown in Fig. 17. Though challenging to solve due to multiple impulses, we use the method proposed in [12] to obtain the impulsive solution using the initial guess obtained from the solution with $a_{\max} = 3.5 \times 10^{-2}$ m/s^2 to obtain a near-impulsive maneuver

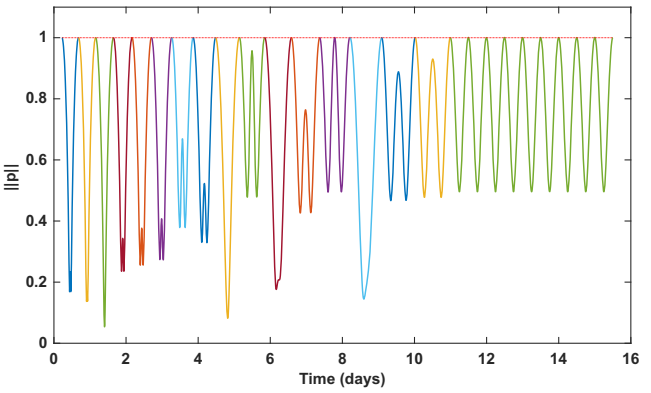

Fig. 19 G2G problem: primer vector magnitude vs time with $N_{\text{rev}} = 21$.

shown in Fig. 18. Figure 19 shows the time history of the primer vector magnitude associated with the converged impulsive solution. The total Δv for this pure impulsive solution came out to be $\Delta v_{\text{total}} = 1.48314461$ km/s.

D. GTO to L1

An even more challenging rendezvous problem of GTO2L1 involving 50 revolutions is solved. The MEE boundary conditions for this maneuver are

$$\boldsymbol{x}_0 = [0.2765649\ (\text{DU}), 0.725, 0, 0.06116262, 0, 0]^{\mathsf{T}},$$
$$\tilde{\boldsymbol{x}}_d = [7.74\ (\text{DU}), 0{,}0{,}0{,}317.3009]^{\mathsf{T}}$$

The equivalent classical orbital elements $(a, \text{ecc}, \text{inc}, \omega, \Omega, \nu)$ defining this transfer are $\boldsymbol{\Psi}_o = [0.583009\ \text{DU}, 0.725, 7\ \text{deg.}, 0, 0, 0]$ and $\boldsymbol{\Psi}_f = [7.74\ \text{DU}, 0, 0\ \text{deg.}, 0, 0, \pi]$. The other parameters are $P_{\text{use}} = 1000$ W, and $m_0 = 240$ kg, $\Delta t = 60$ days, and the number of revolutions is equal to 50. The solution to the unconstrained $c_{\max}$ method displays a continuous thrust profile as depicted in Fig. 20 with a $\Delta v_{\text{total}} = 2.99$ km/s and the largest value of I_{sp} recorded as 2024.42 s. The specific impulse is reduced to an $I_{\text{sp}_{\max}} = 1000$ s before handing over the converged costates and $a_{\max}$ value of 7×10^{-4} m/s^2 to the $a_{\max}$ method. This transition point from the $c_{\max}$ method to the $a_{\max}$ method is arbitrary and was chosen when a slight convergence issue was encountered. The value of $a_{\max}$ is then swept from 7.0×10^{-4} to 8.0×10^{-3} m/s^2, beyond which ΔV does not change significantly (see Fig. 21). As shown in Fig. 22, the final optimal approximate impulsive solution obtained for $a_{\max} = 7.5 \times 10^{-3}$ m/s^2 consists of neither a late departure nor an early arrival with a $\Delta v_{\text{total}} = 1.6608$ km/s and 52 impulses.

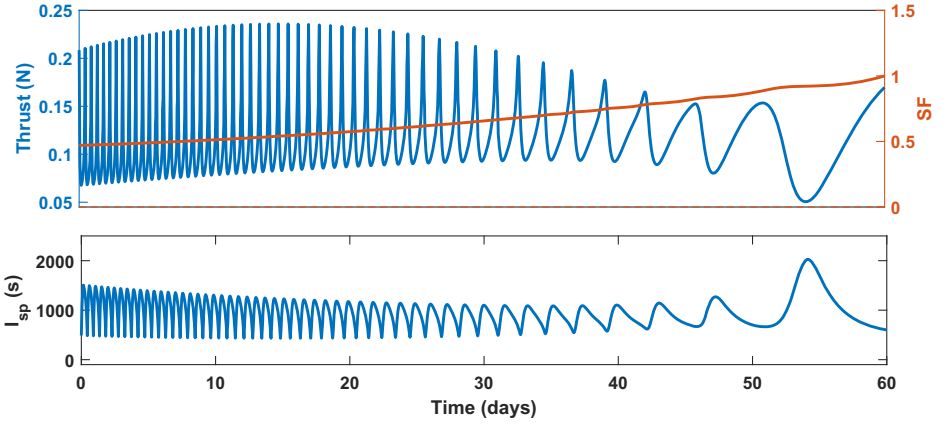

Fig. 20 GTO2L1 problem: optimal thrust and switching function profiles for using unconstrained I_{sp} in the $c_{\max}$ method.

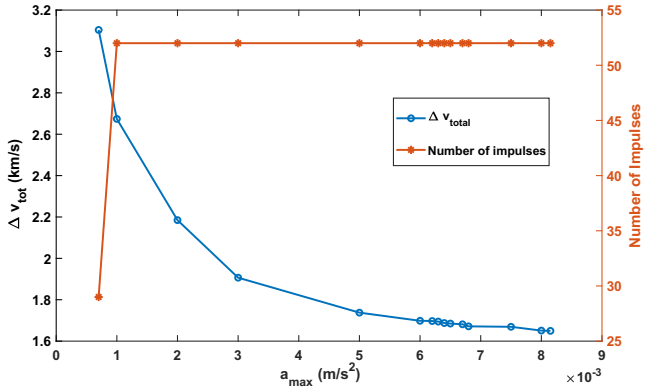

Fig. 21 GTO2L1 problem: ΔV, departure time since the initial epoch, and number of impulses are plotted against the sweeping parameter $a_{\max}$ for the optimal approximate impulsive trajectory.

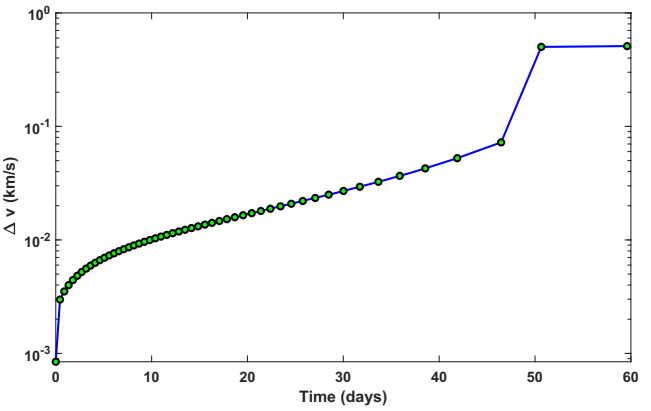

Fig. 23 GTO2L1 problem: Δv distribution for the optimal approximate impulsive trajectory plotted on a log scale against time of impulses.

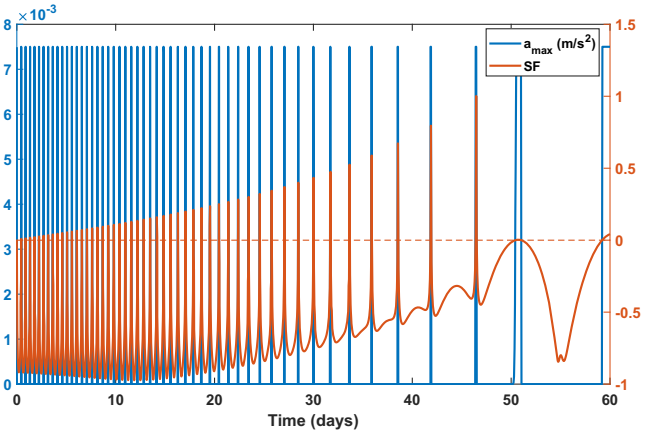

Fig. 24 GTO2L1 problem: acceleration and switching function profiles for $a_{\max} = 7.5 \times 10^{-3}$ m/s^2.

Every orbital revolution consists of a finite burn close to the perigee to raise the semimajor axis. The majority of the expensive inclination change is achieved in the last few orbits when the spacecraft is far from the Earth, which results in large magnitude impulses, as shown in Figs. 23 and 24. This example shows the power of viewing the impulsive case as a limiting case of an indirect function space trajectory optimization approximations. We can solve higher dimensionality minimum impulse problems via the $a_{\max}$ algorithm, which provides a more uniform distribution of impulses that tend to be practically more realizable. The approximate near-impulsive maneuver corresponding to GTO2L1 maneuver is shown in Fig. 25.

IV. Conclusions

Two novel methods are proposed for finding multi-impulse, minimum-ΔV spacecraft maneuvers. The results indicate that both methods are capable of obtaining near-optimal impulsive trajectories for maneuvers with medium levels of complexity. Earth-to-Mars maneuver in this work was easy and fast to solve using both the methods individually, requiring only a couple of iterations. Similarly, a few iterations of either of the methods were sufficient for the Earth-to-Dionysus problem. It is for more complex problems like the two geocentric maneuvers from GTO solved in this work that a two-step process is invoked.

The presented two-step process helps in mitigating the individual shortcomings of both methods to provide a powerful tool that can especially generate complex impulsive maneuvers. In particular, a near-optimal multi-impulse ($N = 52$ impulses), multirevolution (50 revolutions) maneuver is generated using the proposed method. While it is difficult to design a trajectory with many closely occurring impulses in a practical mission, it is informative to obtain theoretically optimal trajectories to serve as a benchmark. In practice, pruning of the smallest impulses will likely be required or desired, which will belong to our future. Additionally, it might be desirable to use a single algorithm for the setup in place of a two-step process, which is also a subject of future work.

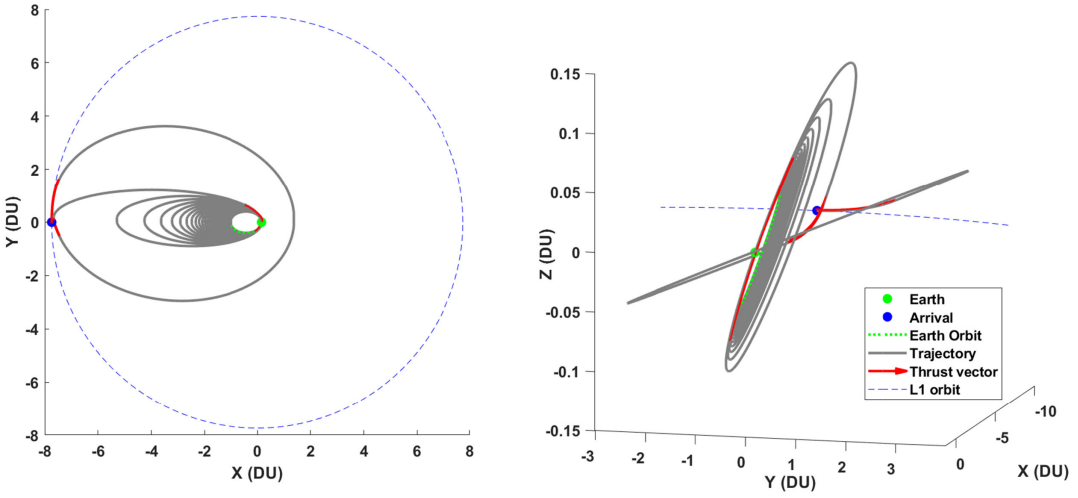

Fig. 22 GTO2L1 problem: optimal approximate impulsive trajectory.

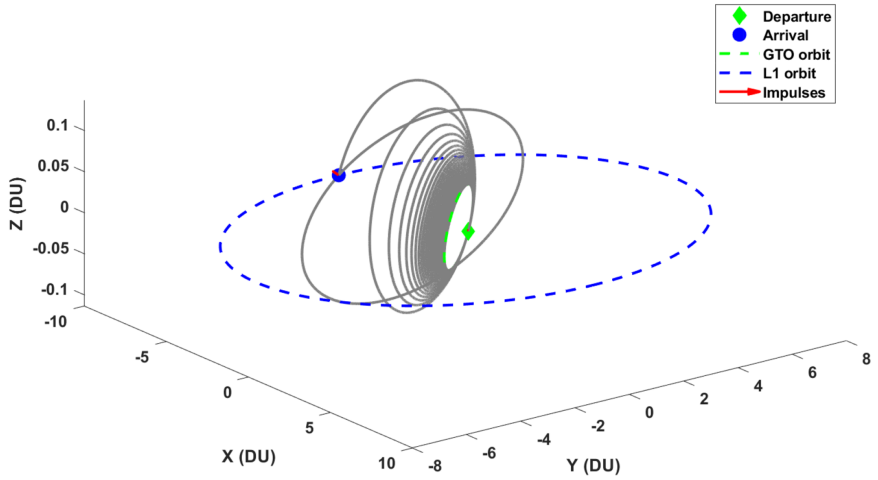

Fig. 25 GTO2L1 problem: impulsive trajectory with $\Delta v = 1.54812$ km/s.

References

[1] Carter, T. E., "Necessary and Sufficient Conditions for Optimal Impulsive Rendezvous with Linear Equations of Motion," *Dynamics and Control*, Vol. 10, No. 3, 2000, pp. 219–227. https://doi.org/10.1023/A:1008376427023

[2] Wen, C., Peng, C., and Gao, Y., "Reachable Domain for Spacecraft with Ellipsoidal Delta-V Distribution," *Astrodynamics*, Vol. 2, No. 3, 2018, pp. 265–288. https://doi.org/10.1007/s42064-018-0025-x

[3] Yang, Z., Luo, Y.-Z., and Zhang, J., "Nonlinear Semi-Analytical Uncertainty Propagation of Trajectory Under Impulsive Maneuvers," *Astrodynamics*, Vol. 3, No. 1, 2019, pp. 61–77. https://doi.org/10.1007/s42064-018-0036-7

[4] Prussing, J. E., "Illustration of the Primer Vector in Time-Fixed, Orbit Transfer," *AIAA Journal*, Vol. 7, No. 6, 1969, pp. 1167–1168.

[5] Lawden, D. F., *Optimal Trajectories for Space Navigation*, Vol. 3, Butterworths, London, 1963, pp. 10–126.

[6] Edelbaum, T., "How Many Impulses?" *3rd and 4th Aerospace Sciences Meeting*, AIAA Paper 1967-0007, 1967.

[7] Luo, Y.-Z., Zhang, J., Li, H.-Y., and Tang, G.-J., "Interactive Optimization Approach for Optimal Impulsive Rendezvous Using Primer Vector and Evolutionary Algorithms," *Acta Astronautica*, Vol. 67, Nos. 3–4, 2010, pp. 396–405. https://doi.org/10.1016/j.actaastro.2010.02.014

[8] Bokelmann, K. A., and Russell, R. P., "Optimization of Impulsive Europa Capture Trajectories Using Primer Vector Theory," *Journal of the Astronautical Sciences*, Vol. 67, No. 2, 2020, pp. 1–26. https://doi.org/10.1007/s40295-018-00146-z

[9] Landau, D., "Efficient Maneuver Placement for Automated Trajectory Design," *Journal of Guidance, Control, and Dynamics*, Vol. 41, No. 7, 2018, pp. 1531–1541. https://doi.org/10.2514/1.G003172

[10] Shirazi, A., Ceberio, J., and Lozano, J. A., "Spacecraft Trajectory Optimization: A Review of Models, Objectives, Approaches and Solutions," *Progress in Aerospace Sciences*, Vol. 102, Oct. 2018, pp. 76–98. https://doi.org/10.1016/j.paerosci.2018.07.007

[11] Shen, H.-X., Casalino, L., and Luo, Y.-Z., "Global Search Capabilities of Indirect Methods for Impulsive Transfers," *Journal of the Astronautical Sciences*, Vol. 62, No. 3, 2015, pp. 212–232. https://doi.org/10.1007/s40295-015-0073-x

[12] Taheri, E., and Junkins, J. L., "How Many Impulses Redux," *Journal of the Astronautical Sciences*, Vol. 67, No. 2, 2020, pp. 257–334. https://doi.org/10.1007/s40295-019-00203-1

[13] Chi, Z., Wu, D., Jiang, F., and Li, J., "Optimization of Variable-Specific-Impulse Gravity-Assist Trajectories," *Journal of Spacecraft and Rockets*, Vol. 57, No. 2, 2020, pp. 291–299. https://doi.org/10.1016/j.ast.2020.105828

[14] Restrepo, R. L., and Russell, R. P., "Shadow Trajectory Model for Fast Low-Thrust Indirect Optimization," *Journal of Spacecraft and Rockets*, Vol. 54, No. 1, 2017, pp. 44–54. https://doi.org/10.2514/1.A33611

[15] Fitzgerald, R. M., "Characterizing Minimum-Time Solar Sail Geostationary Orbit Transfers Using Pseudospectral Optimal Control," *Journal of Spacecraft and Rockets*, Vol. 58, No. 4, 2021, pp. 997–1009. https://doi.org/10.2514/1.A34950

[16] Shannon, J. L., Ozimek, M. T., Atchison, J. A., and Hartzell, C. M., "Rapid Design of High-Fidelity Low-Thrust Transfers to the Moon," *Journal of Spacecraft and Rockets*, Vol. 59, No. 5, 2022, pp. 1522–1535. https://doi.org/10.2514/1.A35177

[17] Taheri, E., Arya, V., and Junkins, J. L., "Acceleration-Based Indirect Method for Continuous and Impulsive Trajectory Design," *31st AAS/AIAA Space Flight Mechanics Meeting*, AAS Paper 21-399, Feb. 2021.

[18] Saloglu, K., and Taheri, E., "Acceleration-Based Switching Surfaces for Impulsive Trajectory Design in Restricted Three-Body Dynamics," *2022 AAS/AIAA Astrodynamics Specialist Conference*, AAS Paper 22-838, Aug. 2022.

[19] Ottesen, D., and Russell, R. P., "Unconstrained Direct Optimization of Spacecraft Trajectories Using Many Embedded Lambert Problems," *Journal of Optimization Theory and Applications*, Vol. 191, Dec. 2021, pp. 634–674. https://doi.org/10.1007/s10957-021-01884-1

[20] Hintz, G. R., "Survey of Orbit Element Sets," *Journal of Guidance, Control, and Dynamics*, Vol. 31, No. 3, 2008, pp. 785–790. https://doi.org/10.2514/1.32237

[21] Haberkorn, T., Martinon, P., and Gergaud, J., "Low Thrust Minimum-Fuel Orbital Transfer: A Homotopic Approach," *Journal of Guidance, Control, and Dynamics*, Vol. 27, No. 6, 2004, pp. 1046–1060. https://doi.org/10.2514/1.4022

[22] Junkins, J. L., and Taheri, E., "Exploration of Alternative State Vector Choices for Low-Thrust Trajectory Optimization," *Journal of Guidance, Control, and Dynamics*, Vol. 42, No. 1, 2018, pp. 47–64. https://doi.org/10.2514/1.G003686

[23] Taheri, E., Junkins, J. L., Kolmanovsky, I., and Girard, A., "A Novel Approach for Optimal Trajectory Design with Multiple Operation Modes of Propulsion System, Part 1," *Acta Astronautica*, Vol. 172, July 2020, pp. 151–165. https://doi.org/10.1016/j.actaastro.2020.02.042

[24] Taheri, E., and Junkins, J. L., "Generic Smoothing for Optimal Bang-Off-Bang Spacecraft Maneuvers," *Journal of Guidance, Control, and Dynamics*, Vol. 41, No. 11, 2018, pp. 2470–2475. https://doi.org/10.2514/1.G003604

[25] Arya, V., Taheri, E., and Junkins, J. L., "A Composite Framework for Co-Optimization of Spacecraft Trajectory and Propulsion System," *Acta Astronautica*, Vol. 178, Jan. 2020, pp. 773–782. https://doi.org/10.1016/j.actaastro.2020.10.007

[26] Casalino, L., and Colasurdo, G., "Optimization of Variable-Specific-Impulse Interplanetary Trajectories," *Journal of Guidance, Control, and Dynamics*, Vol. 27, No. 4, 2004, pp. 678–684. https://doi.org/10.2514/1.11159

[27] Lion, P., and Handelsman, M., "Primer Vector on Fixed-Time Impulsive Trajectories," *AIAA Journal*, Vol. 6, No. 1, 1968, pp. 127–132. https://doi.org/10.2514/3.4452

[28] Prussing, J. E., "Primer Vector Theory and Applications," *Spacecraft Trajectory Optimization*, Vol. 29, Cambridge Univ. Press, Cambridge, England, U.K., 2010, p. 16.

[29] Taheri, E., Kolmanovsky, I., and Atkins, E., "Enhanced Smoothing Technique for Indirect Optimization of Minimum-Fuel Low-Thrust Trajectories," *Journal of Guidance, Control, and Dynamics*, Vol. 39, No. 11, 2016, pp. 2500–2511. https://doi.org/10.2514/1.G000379

[30] Arya, V., Taheri, E., and Junkins, J., "Hyperbolic Tangent-Based Smoothing with State Transition Matrix Implementation for Generating Fuel-Optimal Trajectories," *29th AAS/AIAA Space Flight Mechanics Meeting*, AAS Paper 19-496, Jan. 2019.

[31] Ross, I. M., Gong, Q., and Sekhavat, P., "Low-Thrust, High-Accuracy Trajectory Optimization," *Journal of Guidance, Control, and Dynamics*, Vol. 30, No. 4, 2007, pp. 921–933. https://doi.org/10.2514/1.23181

C. N. McGrath
Associate Editor